

Application of the carré algorithm and high speed interferometer technique for fast surface profile measurement

DAVID ASAEL GUTIÉRREZ HERNÁNDEZ*, CARLOS PÉREZ LÓPEZ, FERNANDO MENDOZA SANTOYO
Centro de Investigaciones en Óptica. Lomas del Bosque 115. Col. Lomas del Campestre. C.P. 31715. León, Guanajuato, México

The measurement of a surface profile by using High Speed Electronic Speckle Pattern Interferometry (HS-ESPI) is presented. It is realized by the temporal phase shifting algorithm proposed by Carré. The HS-ESPI is configured to 4000 frames per second (fps). Traditionally, temporal phase shifting techniques employed piezoelectric components to retrieve the optical phase of the measured object. In this work the retrieved optical phase comes directly from the object itself which is under a vibration condition. The measurement is done without the need of any piezoelectric component, any electronic synchronization or any other external component.

(Received October 28, 2013; accepted March 13, 2014)

Keywords: ESPI, High Speed Interferometry, Vibrations

1. Introduction

Phase measurement techniques have been used to directly measure wavefront phase in an interferometer as long as a relative difference between the object beam and the reference beam exists. Those techniques which take the phase data sequentially are called Temporal Phase Measurement and those which take the phase data simultaneously are known as Spatial Phase Measurements [1]. To determine phase, electronic and analytic techniques are used. The analytic techniques have become more popular between researches because of the use of a computer to process the information. Different analytical algorithms have been published along the time working with a set of three, four or five recorded fringe patterns with a phase shift of $\pi/2$, however, there have been developed algorithms that are independent of the amount of phase shift [2-9] where their applications result more interesting for measurements done in different fields of industry. Recent works have reported new methods that describe new algorithms for phase recovery with just one or two steps [10-15]. The application of these algorithms requires of a phase change in the reference beam by means of a tilted mirror or another transducer. In this work, the change of phase comes directly from the excited object due to a natural vibration mode. The Carré algorithm, established in 1966 [2], is applied to a selected group of fringe patterns coming from the HS-ESPI system, where a continuous wave laser illumination and a high speed camera are used.

2. Experimental setup and object description

The optical set-up for this experiment is an out-of-plane sensitive ESPI, shown in Fig. 1. A continuous beam coming from a laser source with a maximum power source of 6 Watts and 532 nm wavelength, is divided by the beam splitter (BS1), into an object (I_O) and a reference (I_R) beams. MO1 is a 10x microscope objective that projects the object beam over the target. MO2 is a 10x microscope objective that projects the reference beam over the camera sensor through a beam splitter, BS2, which also recombines the reflected intensity coming from the object into the camera, which is a CMOS NAC's Memrecam fx 6000. For this work, in order to get the most possible information of the event to measure, the laser is set to a power of 5.5 Watts and the CMOS camera is set to an exposure time of 4000 frames per second leaving the shutter permanently open. It was seen that there is a relation between the power of the laser and the exposure time of the camera, if more frames per second are recorded, more power is needed.

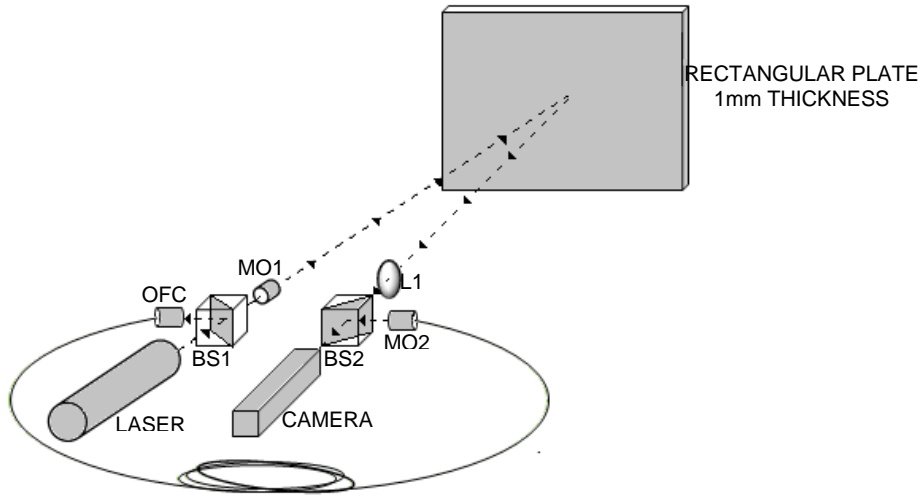


Fig. 1. Optical set up for a high-speed ESPI system. Beam splitter 1 is a 70/30, beam splitter 2 is a 50/50, microscope objectives are 10x. The material properties of the 6061 aluminum alloy plate are mass density $\rho = 2700 \text{ kg/m}^3$, Young's modulus $E = 70 \text{ GPa}$ and the Poisson ratio $\nu = 0.33$, according to the aluminum standards and data 2006 Metric SI by the Aluminum Association Inc.

The rectangular plate is clamped in its four edges with a distributed load. The plate is excited at its first modal vibration which was found at 320 Hz. The excitation is produced by an external sine wave generator plugged to a conventional speaker placed behind the plate. L1 has a focal length of 75mm and helps the system to capture the full area of the plate and record the evolution of the vibration by the high-speed CMOS camera.

The rectangular plate under vibration has been studied by [16-20] where it is found that the classical differential equation of motion for the transverse displacement or deflection function $u(x, y, t)$ of an isotropic homogeneous thin plate is given by the fourth order differential equation

$$D\nabla^4 u + \rho \partial^2 u / \partial t^2 = p \quad (1)$$

Where $\nabla^4(\) \equiv \frac{\partial^4}{\partial x^4} + 2\frac{\partial^4}{\partial x^2 \partial y^2} + \frac{\partial^4}{\partial y^4}$ is commonly called the biharmonic operator. The flexural rigidity of the plate, D , can be expressed by $D = \frac{Eh^3}{12(1-\nu^2)}$, where E is the Young's modulus, h is the thickness of the plate and ν is the Poisson ratio.

$\partial^2 u / \partial t^2 = c^2 \left(\partial^2 u / \partial x^2 + \partial^2 u / \partial y^2 \right)$ where c is an elastic constant that depends on the mechanical properties of the material, and p is the distributed load. The deflection function, $u(x, y, t)$, must satisfy the border conditions $u = 0$ for all $t > 0$.

In the simpler case of a plate with its edges simply supported, the bending moments are zero and it is possible to express the transverse displacement as a product of sine functions, as it is written in equation (2), where a corresponds to the length and b to the width for each horizontal and vertical vibration modal, w and z respectively. According to [21, 22], it has relied on the assumption that, far from the boundaries, a clamped plate has similar mode shapes to those of a simply supported plate.

$$u_{wz}(x, y, t) = C \sin(w\pi/a) \sin(z\pi/b) \quad (2)$$

In which the constant C must be chosen so as to satisfy Eq. (1) where p must be written as

$$p = p_0 \sin \frac{w\pi}{a} \sin \frac{z\pi}{b} \quad (3)$$

in which p_0 represents the intensity of the load at the center of the plate.

Fig. 2 shows the principal numerical analysis of the rectangular plate through a simulation with $a = 19$ and $b = 14$. The deformed profile of the vibrating plate on its first natural mode of frequency fits a parabolic function.

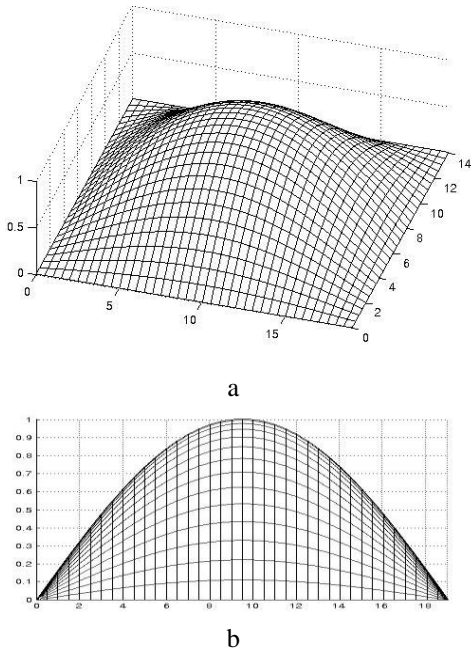


Fig. 2. (a) Numerical model for a modal vibrating rectangular plate with length, $a = 19$, and width, $b = 14$, the z -axis represents the normalized deflection of the plate, (b) profile of the dynamic deformation of the plate.

3. Theoretical description

It is observed from Fig. 1 that the laser source is divided into 2 beams, I_R and I_O . Both beams are recombined on the CMOS sensor. This recombination can be written by the expression

$$I_1 = I_O + I_R + 2\sqrt{I_O I_R} \cos(\Psi) \quad (4)$$

where Ψ is the subtraction of the phase of the wavefront of the object beam, ϕ_O , and the phase of the wavefront of the reference beam, ϕ_R .

Once the surface of the object is deformed, a change of phase, $\Delta\phi$, is introduced as follows,

$$I_2 = I_O + I_R + 2\sqrt{I_O I_R} \cos(\Psi + \Delta\phi) \quad (5)$$

The subtraction of intensities of the input images I_1 and I_2 can be given by

$$|I_1 - I_2| = 4\sqrt{I_O I_R} \sin\left(\Psi + \frac{1}{2}\Delta\phi\right) \sin\left(\frac{1}{2}\Delta\phi\right) \quad (6)$$

Eq. (6) represents a fringe pattern that can be numerically processed to obtain a phase map for measuring the deformation of the object. A detailed theory

of the operation of the electronic speckle pattern interferometer can be found in [23, 24].

When a sinusoidal signal produces an oscillated vibration on the surface of the object, the phase change $\Delta\phi$ can be expressed as

$$\Delta\phi = \frac{4\pi}{\lambda} A \sin \omega t \quad (7)$$

where λ is the wavelength of a laser, A is the amplitude of the signal and ω is the natural frequency of vibration. This equation indicates that the deformation on the object's surface will change cyclically going through minimum and maximum values of the amplitude A . For this case, it is considered that with the HS-ESPI system there are more than two intensities that can be stored by the sensor while the object is under deformation, in this specific case, 4000 intensities going from $I_1, I_2, I_3, \dots, I_n$, with a phase change going between 0 and 2π once and over until covering 12 cycles of vibrations as it was described above.

The number of intensity patterns stored in a complete vibration cycle will depend on the natural frequency, ω , and on the exposure time of the CMOS camera, τ .

In this case, the intensity patterns stored by the camera can be written as

$$I_n(x, y) = I_O(x, y) + I_R(x, y) + 2\sqrt{I_O(x, y)I_R(x, y)} \cos\left(\psi(x, y) + \frac{2(n-1)\pi}{m}\right) \quad (8)$$

where m is the number of fringe patterns that can be obtained by the relation between the exposure time of the camera and the vibration frequency of the plate, it can be calculated from $m \approx \text{int}[\tau\omega^{-1}]$ and $n = 1, 2, 3, 4, 5, 6, \dots, m$. The integer function $\text{int}[\]$ gives an integer number of fringe patterns that can be used in the proposed method and allows the selection of the fringe patterns with the same amount of phase shifts between them.

The subtraction of intensities of the input images I_1 and I_2 to I_n can be given by

$$|I_1(x, y) - I_n(x, y)| = 4\sqrt{I_O(x, y)I_R(x, y)} \sin\left(\psi(x, y) + \frac{(n-1)\pi}{m}\right) \sin\left(\frac{(n-1)\pi}{m}\right) \quad (9)$$

Each of these subtractions represents a fringe pattern. With this information, the reconstruction of the deformation during a complete vibration cycle of the object can be done.

One of the most important considerations of this technique is that the measurement can be started at any time; it is only needed to select an intensity pattern and make a subtraction of the following consecutive intensity

patterns to it. It is not need of any kind of synchronization or any kind of carrier to do the measurement.

Some of the phase shifting techniques requires a particular and exact amount of phase change between consecutive intensity measurements in order to apply specific algorithms for phase calculation. Carré [2] presented in 1966 a technique of phase measurement which is independent of the amount of phase shift between consecutive measurements, yielding four equations,

$$I_1(x, y) = I_0(x, y) \left[1 + \gamma(x, y) \cos \left(\phi(x, y) - \frac{3\alpha}{2} \right) \right] \quad (10)$$

$$I_2(x, y) = I_0(x, y) \left[1 + \gamma(x, y) \cos \left(\phi(x, y) - \frac{\alpha}{2} \right) \right] \quad (11)$$

$$I_3(x, y) = I_0(x, y) \left[1 + \gamma(x, y) \cos \left(\phi(x, y) + \frac{\alpha}{2} \right) \right] \quad (12)$$

$$I_4(x, y) = I_0(x, y) \left[1 + \gamma(x, y) \cos \left(\phi(x, y) + \frac{3\alpha}{2} \right) \right] \quad (13)$$

where the phase shift, α , is assumed to be linear. I_0 is the background intensity, γ is the fringe modulation, $\phi(x, y)$ is the phase distribution to be measured. From these equations, the phase shift can be calculated by means of,

$$\alpha = 2 \tan^{-1} \left[\frac{\sqrt{3(I_2 - I_3) - (I_1 - I_4)}}{(I_2 - I_3) + (I_1 - I_4)} \right] \quad (14)$$

where the phase at each point is calculated by

$$\phi = \tan^{-1} \left\{ \tan \left(\frac{\alpha}{2} \right) \frac{(I_1 - I_4) + (I_2 - I_3)}{(I_2 + I_3) - (I_1 + I_4)} \right\} \quad (15)$$

Combining the above two equations, the phase module π can be calculated by,

$$\phi = \tan^{-1} \left\{ \frac{\sqrt{[(I_1 - I_4) + (I_2 - I_3)][3(I_2 - I_3) - (I_1 - I_4)]}}{(I_2 + I_3) - (I_1 + I_4)} \right\} \quad (16)$$

Equation (16) determines the phase module π at each point in the interferogram without phase calibration errors.

The fringe modulation for this technique is

$$\gamma = \frac{1}{2I_0} \sqrt{\frac{[(I_1 - I_4) + (I_2 - I_3)]^2 + [(I_2 + I_3) - (I_1 + I_4)]^2}{2}} \quad (17)$$

4. Simulating results

For this experiment, the vibration frequency of the plate is $\omega = 320\text{Hz}$ and the CMOS camera is set to an

exposure time, $\tau = 4000\text{fps}$, so, there are 12 intensity patterns recorded for a complete cycle of vibration and 12 complete cycles recorded in 4000 fps. All of them must satisfy the theoretical deformation description fitting a parabolic function as it was described above. In this work, only one cycle is considered in order to demonstrate the application of the Carré algorithm.

The intensity patterns are separated from each other by a constant phase shift, α . The fringe patterns obtained by the subtraction of the intensity patterns are shown in Fig. 3. The figure represents a complete cycle of vibrating evolution where the maximum deformation of the plate is located in the center of it.

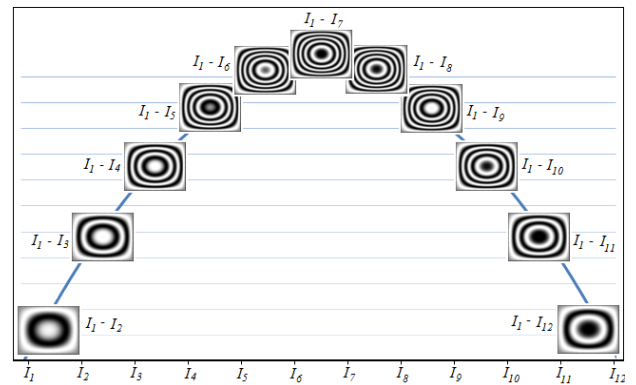


Fig. 3. Full vibration cycle and its theoretical fringe pattern evolution. The y-axis measures the relative deformation amplitude and the x-axis shows the interferograms at different phase and time positions.

According to the Carré technique, a fringe pattern is phase shifted by, for example, a tilting a mirror to get 4 different fringe patterns to be applied in equations (10) to (13), in other words, the tilting mirror changes the phase to $\Delta\phi$ equals to $0, \pi/2, \pi$ and $3\pi/2$. For this experiment, the phase change comes from a surface displacement due to equation (7), in this case, it can be considered that

$$\Delta\phi = \frac{4\pi}{\lambda} A \sin \omega t = 0, \frac{\pi}{2}, \pi, 3\frac{\pi}{2}, 2\pi \quad (18)$$

where $A \sin \omega t = 0, \frac{\lambda}{8}, \frac{\lambda}{4}, 3\frac{\lambda}{8}, \frac{\lambda}{2}$, respectively. This

indicates that a phase change as a result of a mirror position is equivalent to the optical phase change coming from a displacement of the surface of the plate. With this assumption, it is possible to detect 4 fringe patterns coming from only one cycle of vibration and applied a well-known algorithm in order to measure a phase. This is because the HS-ESPI allows to measure the evolution of the vibration cycle along the time with several samples, which can be interpreted as a phase stepping technique, as shown in Fig. 4.

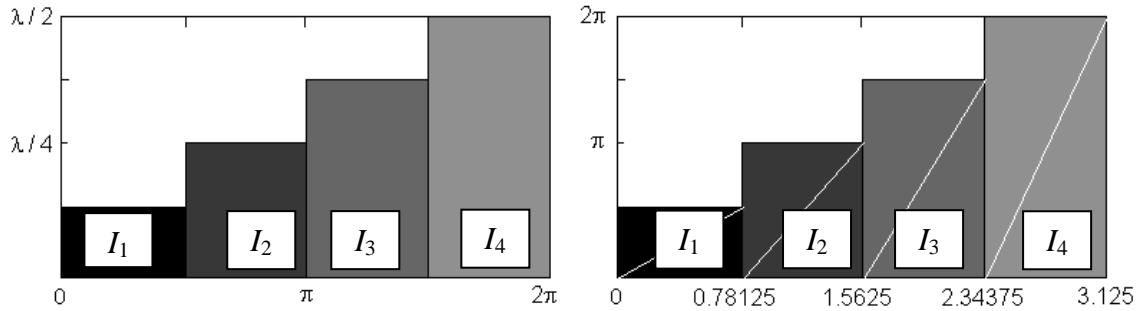


Fig. 4. Phase stepping in HS-ESPI in a cycle of vibration a) x-axis is the phase shift (time) and y-axis is the intensity change coming from the displacement of the plate; b) equivalent interpretation of phase stepping with HS-ESPI. X-axis is the time in ms and y-axis is the phase change.

According to Fig. 3, there are 11 fringe patterns in a complete cycle of vibration. Each fringe pattern is formed

at a specific time within the cycle as shown in Fig. 5.

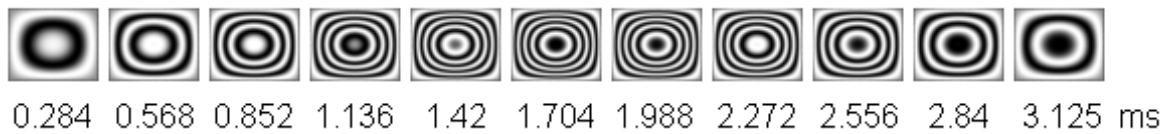


Fig. 5. Fringes patterns contended in a cycle of vibration.

The selected fringe patterns along the complete vibration cycle are shown in Fig. 6.

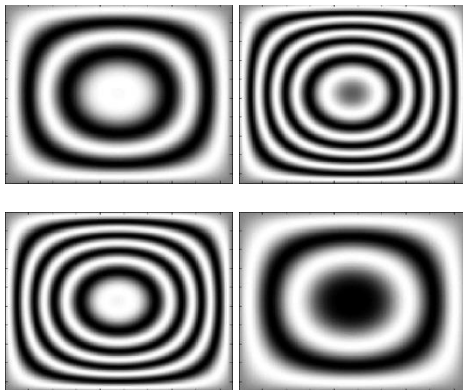


Fig. 6. 4 images are selected for applying the Carré's algorithm. Each image corresponds to 0.568, 1.42, 2.272 and 3.125 ms respectively.

For this experiment these fringe patterns are separated from each other by an amount of phase $\alpha = 6\pi/11 = 98.18^\circ$.

Once the fringes are processed by eq. (16), the resulted wrapped phase is then computationally unwrapped by the weighted multigrid method [25]. The unwrapped phase map and the profile along the center of it, in the x-axis direction, are shown in Fig. 7.

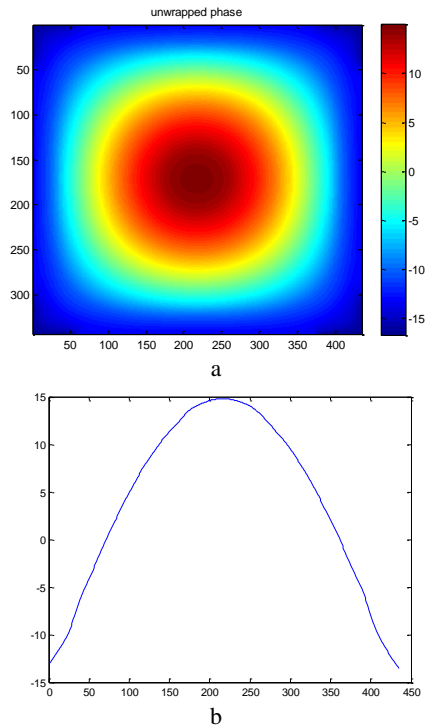


Fig. 7. a) Recovered phase of the rectangular plate under deformation. x and y axis are pixels; b) profile of the deformation of the vibrating plate that comes from the processing of 4 selected fringe patterns with an amount of phase $\alpha=98.18^\circ$ ($\alpha=6\pi/11$) between each other, x-axis is in pixels and y-axis is in radians.

The computational and mathematical processing for this work is done with a software [26] based on Matlab instructions.

According to [27], it is important to mention that the four fringe patterns have to be selected along the deformation and must keep the same amount of phase shifts between each other. Otherwise, the method wouldn't work properly.

5. Experimental results

The experimental fringe patterns coming by the HS-ESPI are shown in Fig. 8. There is a very visible noise that looks like a group of horizontal lines. This phenomenon is due to manufacturing problems specifically for this model camera. According to the manufacturer, this error was corrected for subsequent versions. The camera's version is the NAC's Memrecam fx 6000, however, this phenomenon doesn't affect the measurement because it is a constant noise and not a phase changing.

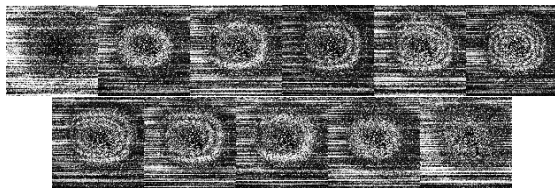


Fig. 8. Full vibration cycle and its fringe pattern evolution. The images are in a gray level scale at 8 bits.

The four fringe patterns selected to be processed with the Carré algorithm with an amount of phase of 98.18° are:

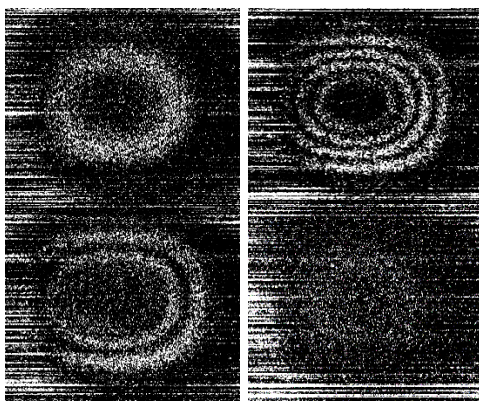
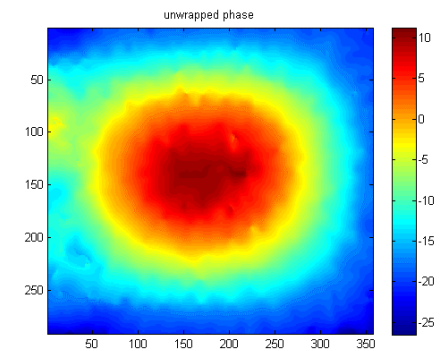
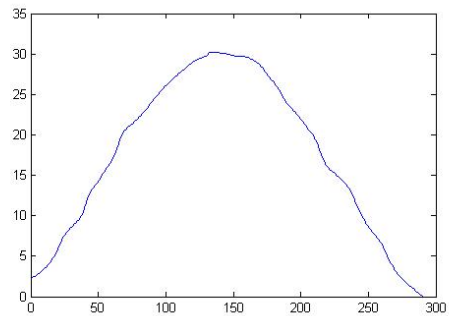


Fig. 9. The selected fringe patterns to be processed by eqn. (16). The images correspond to a phase changes of $4\pi/11$, $10\pi/11$, $16\pi/11$, 2π .

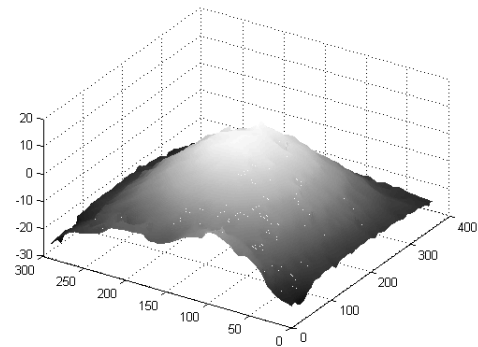
Once the eqn. (16) is applied, the resulted wrapped phase is then unwrapped by the weighted multigrid method. The resulted unwrapped phase map is shown in Fig. 10 as well as the profile along the center of it in the y-axis direction.



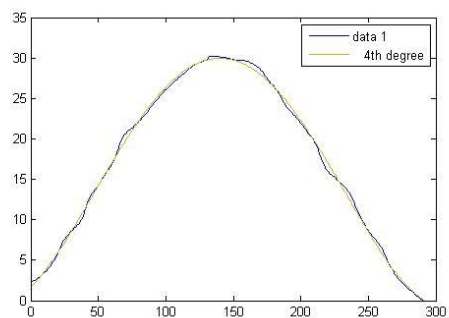
a



b



c



d

Fig. 10. (a) Recovered unwrapped phase of the experimental work; (b) Experimental profile of the deformation of the rectangular plate that comes from the processing of 4 selected fringe patterns with an amount of phase $\alpha=98.18^\circ$ between each other. x-axis is in pixels and y-axis is in radians; (c) 3D graph of the results obtained; (d) comparative plot between the theoretical and experimental profile.

For this experiment, the adjustment of the profile shown in Fig. 10 (d) to a parabolic function is equal to 0.9983. It means that the experimental profile measured on this work fits the theoretical modelling described above. This result indicates that the combination of Carré and HS-ESPI methods works without the need of any synchronization between techniques and without the need of a mechanical tilt of a component for shifting an amount of phase in the experiment.

The mechanical amplitude of the deformation for the profile that is shown in Fig. 10 (b) can be calculated by means of equation (7), so, the deformation on the maximum point of the experimental profile measured is equal to $0.727\mu\text{m}$.

Different vibration frequency will involve a different exposure time on the camera. We work at 320Hz [28], which is the first vibration natural mode of the rectangular plate. The relation between the exposure time and the vibration frequency gives enough fringe patterns that can be used in the proposed method and ensure that we can measure a complete vibration cycle.

5. Conclusions

A big advantage of Carré technique refers to the not need of phase shift calibration, in this way, the HS-ESPI system working together to the Carré technique is a very fast way to measure mechanical deformation from optical phase changes coming from a vibrating object. The introduction of a high speed camera to an ESPI set up eliminates the need for tilted mirrors or piezoelectric devices to change the phase and also eliminates the need of electronically synchronization. High speed cameras and continuous wave lasers together with optical interferometer systems give a very strong way for measuring real time vibrations with the only need of a complete vibration cycle; its application in industry can be a very interesting solution for complex measurements. The system records a sequence of 4000 fps, which can be used for applying some of the phase shifting techniques proposed from many authors and can be useful to characterize the complete vibration evolution of a dynamic event.

Acknowledgments

The authors would like to acknowledge partial financial support from Consejo Nacional de Ciencia y Tecnología, Grant 157594.

References

- [1] H. Helmers, J. Burke, *proc. SPIE* **3744**, 188 (1999).
- [2] P. Carré, *Metrologia* **2**(1), 13 (1966).
- [3] M. Takeda, H. Ina, S. Kobayashi, *J. Opt. Soc. Am.* **72**(1), 156 (1982).
- [4] Y. Y. Cheng, J. C. Wyant, *Appl. Opt.* **24**(18), 3049 (1985).
- [5] P. Hariharan, *Appl. Opt.* **26**, 2504 (1987).
- [6] C. Roddier, F. Roddier, *Appl. Opt.* **26**(9), 1668 (1987).
- [7] K. Creath, *Progress in Optics*, **26**, 350-393, E. Wolf, ed., North Holland, Amsterdam (1988).
- [8] D. Kerr, F. Mendoza Santoyo, J. R. Tyrer, *J. Opt. Soc. Am. A*, **7**, 820 (1990).
- [9] K. A. Goldberg, J. Bokor, *Appl. Opt.* **40**(17), 2886 (2001).
- [10] Q. Yu, S. Fu, X. Liu, X. Yang, X. Sun, *Opt. Express* **12**(20), 4980 (2004).
- [11] J. A. Quiroga, J. A. Gómez-Pedrero, M. J. Terrón-López, M. Servin, *Optics Communications*, **253**, 266 (2005).
- [12] X. H. Zhong, *Appl. Opt.* **45**(35), 8863 (2006).
- [13] Hyun-Jin Lee, Sang-Keun Gil, *J. Opt. Soc. Korea* **10**, 118 (2006).
- [14] Fuzhong Bai, Changhui Rao, *Optics Express*. **17**(19), 16861 (2009).
- [15] Seok-Hee Jeon, Sang-Keun Gil, *J. Opt. Soc. Korea* **15**, 244 (2011).
- [16] D. Young, *Journal of Applied Mechanics*, **62**, A139 (1940).
- [17] T. H. Evans, *Journal of Applied Mechanics*, **61**, A7 (1939).
- [18] I. A. Wojtaszak, *Journal of Applied Mechanics*, **59**, A173 (1937).
- [19] S. P. Timoshenko, In *Proceedings Fifth International Congress of Applied Mechanics*, pages 40-43, Massachusetts Institute of Technology (1938).
- [20] C. E. Imrak, I. Gerdemeli, *Applied mathematical sciences*, **1**, 43, 2129 (2007).
- [21] N. Yoshihiro, *Doctoral thesis, Hokkaido University*, December (1979).
- [22] E. Ventesel, T. Krauthammer, Marcel Dekker, Inc. New York (2001).
- [23] R. Jones, C. Wykes, Cambridge University Press, Cambridge, (1987), 2nd Ed.
- [24] K. Høgmøen, H. M. Pederson, *J. Opt. Soc. Am.*, **67**, 1578 (1977).
- [25] M. D. Pritt, *IEEE transactions on geoscience and remote sensing*, **34**(3), 728 (1996).
- [26] J. Antonio Quiroga, Daniel Crespo J. A. Gomez-Pedrero, *Proc. of SPIE*, **6616**, 66163Y1-10 (2007).
- [27] Q. Kema, S. Fangjun W. Xiaoping, *Meas. Sci. Technol.* **11**, 1220 (2000).
- [28] A. Moore, C. Pérez-López, *Opt. Eng.* **35**(9), 2641 (1996).

*Corresponding author: dgutierrez@ipn.mx